Acta Sci. Pol.
Architectura 25 (2026), 54–73
aspa.sggw.edu.pl ISSN 1644-0633 (suspended) eISSN 2544-1760 DOI: 10.22630/ASPA.2026.25.4

ORIGINAL PAPER

Received: 08.03.2026
Accepted: 03.04.2026

TEMPORAL EVOLUTION OF CLEAR-WATER LOCAL SCOUR DOWNSTREAM OF A WEIR

Julia Górka[1], Marta Kiraga[2]✉

[1] Faculty of Civil and Environmental Engineering, Warsaw University of Life Sciences – SGGW, Warsaw, Poland
[2] Institute of Civil Engineering, Warsaw University of Life Sciences – SGGW, Warsaw, Poland

ABSTRACT

This study investigates the temporal evolution of local scour downstream of a weir under clear-water conditions. The research hypothesis assumes that the majority of scour develops during the initial flow phase and that the rate of scour is influenced by downstream flow velocity. Laboratory experiments were conducted on a 1 : 30 physical model of a damming weir, reproducing realistic sediment and structural conditions. Results show that, on average, 85–86% of the maximum scour depth forms within the first 0.5 h, while subsequent growth slows and stabilises near the final depth. Higher flow velocities accelerate initial scour development but have little effect on later stages. The study confirms the typical clear-water scour pattern and provides quantitative insights useful for assessing structural safety and designing bed protection measures downstream of weirs.

Keywords: local scour, weir, temporal evolution, physical model, hydraulic structure

INTRODUCTION

Hydraulic structures such as weirs, dams, and spillways significantly modify natural flow conditions in rivers. The concentration of flow and the formation of high-velocity jets downstream of such structures frequently lead to intensive bed erosion. Local scour developing in the downstream reach is considered one of the main factors affecting the structural safety and long-term stability of hydraulic infrastructure. Excessive scour may result in exposure of foundations, structural damage, and, in extreme cases, even failure of the structure. For this reason, understanding the mechanisms controlling the development of local scour is an important issue in hydraulic engineering and river management.

Local scour downstream of weirs is one of the most important morphodynamic processes affecting the stability and safety of hydraulic structures (Tunas et al., 2024; Panthi et al., 2026). It results from the interaction between the high-energy jet issuing from the structure, turbulent flow structures, and the erodibility of the bed material. Depending on sediment transport conditions in the approach channel, two basic scour regimes can be distinguished: clear-water scour and live-bed scour. These regimes differ primarily in the presence or absence of sediment transport upstream of the structure and in the mechanisms controlling the equilibrium depth of scour (Fig. 1). It should be noted that Figure 1 is a simplified schematic intended solely to illustrate sediment transport processes and scour development. The depicted water levels and overflow heights do not represent exact physical measurements but are exaggerated for clarity of the conceptual explanation.

Marta Kiraga https://orcid.org/0000-0001-9729-4209
✉marta_kiraga@sggw.edu.pl

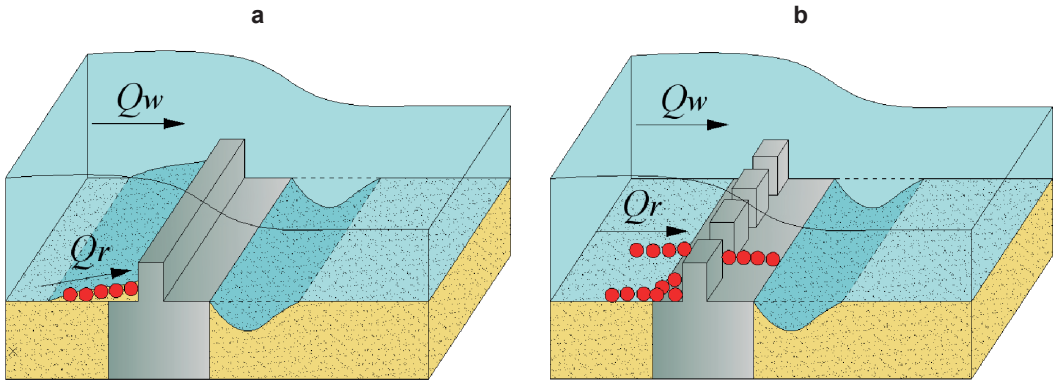

Fig. 1. Local scour downstream of a weir under different clear-water (a) and live-bed (b) sediment transport conditions: Q_w – water discharge, Q_r – sediment transport rate

Source: own work.

Clear-water scour occurs when the mean flow velocity in the upstream channel is lower than the critical velocity required to initiate sediment motion. Under these conditions, the bed material upstream of the weir remains immobile and no sediment is transported into the downstream reach. Consequently, the scour process downstream of the structure develops solely due to the erosive action of the high-velocity jet leaving the weir (Guan et al., 2019; Zhang et al., 2025). The formation of a scour hole typically proceeds through several stages. As the flow passes over the crest or under a gate, it accelerates and forms a high-velocity jet. Upon entering the downstream reach, the jet impinges on the bed, generating strong turbulence and high local shear stresses. Progressive removal of bed material leads to the formation of a scour hole downstream of the structure (Millar et al., 2024). As the scour hole deepens, the geometry of the flow changes and a recirculation zone develops, which transports the eroded material further downstream (Graf, 1989; Guan et al., 2014). The scour process continues until the bed shear stress within the scour hole decreases below the critical value required to mobilise sediment particles. At this stage, sediment motion ceases and the scour depth stabilises, resulting in a static equilibrium configuration (Hopfinger et al., 2004). Clear-water scour is typically characterised by relatively large equilibrium scour depths, since there is no sediment supply from upstream to partially fill the developing scour hole (Ghani & Mohammadpour, 2016; Guan et al., 2019; Fig. 2a).

Live-bed scour (Fig. 2b) occurs when the flow velocity in the approach channel exceeds the critical velocity for sediment motion, meaning that sediment transport already takes place upstream of the weir (Graf, 1989; Guan et al., 2019). In this regime, bed material is continuously transported toward the structure and supplied to the downstream reach. Bed material is transported in the form of bedload and suspended load before reaching the structure. The high-energy jet issuing from the structure erodes the bed material in a manner similar to the clear-water case, producing strong turbulence and local bed degradation (Hopfinger et al., 2004; Guan et al., 2014). The incoming sediment partially deposits within the developing scour hole while part of the material is transported further downstream. As a result, the bed morphology in this zone is continuously changing. The equilibrium scour depth is reached when the rate of sediment removal due to the jet equals the rate of sediment supply from upstream. Unlike the clear-water case, this equilibrium is dynamic and the bed elevation may fluctuate around an average value over time (Fig. 2c). Live-bed scour holes are usually shallower than those formed under clear-water conditions, but they tend to exhibit greater temporal variability due to the continuous sediment transport (Brath & Montabari, 2000).

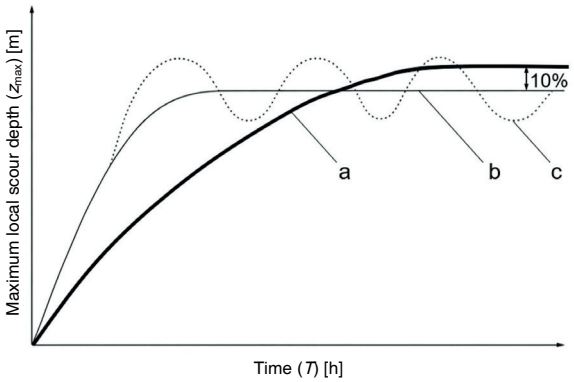

Fig. 2. The course of maximum local scour depth over time in clear-water (a) and live-bed (b) conditions, with visible temporal fluctuations in live-bed scour depth (c)

Source: own work.

Local scour downstream of hydraulic structures has been widely investigated through laboratory experiments, field observations, and numerical modelling. Previous studies have focused on identifying the key parameters controlling scour depth, such as flow velocity, tailwater depth, sediment size, jet characteristics, and the geometry of the structure (Guan et al., 2016; Wang et al., 2018; Lantz et al., 2022; Kiraga et al., 2025; İkincioğulları et al., 2026). Despite the large body of research, predicting the temporal evolution of scour holes remains challenging due to the complex interaction between turbulent flow structures and movable bed processes.

Although many studies have analysed equilibrium scour depth, fewer investigations focus on the temporal development of scour and the relative contribution of different phases of the erosion process. Understanding how quickly the scour hole develops and how the rate of erosion changes over time is particularly important for evaluating the stability of hydraulic structures during flood events.

Therefore, the aim of this study is to analyse the temporal evolution of local scour downstream of a weir under clear-water conditions based on laboratory experiments conducted on a scaled physical model. Special attention is given to the rate of scour development and the contribution of successive phases of the erosion process to the final scour depth.

MATERIAL AND METHODS

Field studies

During the initial phase of the research, a representative hydraulic structure was selected to serve as a prototype for subsequent laboratory investigations. The selected object was a damming weir (Fig. 3) on the Radomka in Piaseczno near Radom (central Poland). The Radomka is a small lowland river with a total length of about 100 km and a catchment area of about 2,000 km^2.

The selection of the structure was based on several criteria. The primary consideration was the feasibility of reproducing the structure within the available laboratory facilities while maintaining appropriate geometric similarity. Additional factors included the structural configuration of the weir, accessibility of the site for field inspections, and the suitability of the structure for analysing hydraulic processes typical of lowland river systems.

Fig. 3. The damming weir on the Radomka in Piaseczno: a – downstream view, b – upstream view of the structure with the impounded water level

Source: Majewska (2025).

To obtain detailed information about the prototype structure and its operating conditions, field inspections were conducted in 2022 and 2024. These site visits allowed for an assessment of the structural layout, technical condition, and hydraulic performance of the weir under natural conditions.

The analysed structure is a monolithic reinforced concrete dock-type weir. The spillway section is divided into three spans separated by two intermediate piers. The principal geometric parameters include a spillway opening width of 5.00 m, a total crest width of 16.50 m, a footbridge width of 4.45 m, a communication walkway width of 1.00 m, and intermediate piers with a width of 0.80 m and a length of 6.35 m.

Laboratory experiment

Based on in situ measurements of the prototype structure, a scaled physical model of the movable weir with three bays, each equipped with sluice gates, was designed and constructed in the Hydraulic Laboratory of the Warsaw University of Life Sciences (SGGW) in Warsaw. The model included structural components such as abutments and piers with rounded edges, mounted on a foundation slab, as well as a threshold with a chamfered downstream edge. The dimensions of the remaining model elements were adjusted to fit the laboratory flume with a fixed cross-section. The finalised dimensions of the individual structural elements are summarised in Table 1. Three-dimensional visualisation of the structure is shown in Figure 4. The model, reproduced at a geometric scale of 1 : 30, allowed detailed investigation of the hydraulic processes associated with the weir under controlled laboratory conditions.

Table 1. Dimensions of the structural elements of the model

Structural element	Number	Dimensions [m]		
		width	length/thickness	height
Semicircular pier	2	0.035	0.518	0.230
Foundation slab	1	0.580	0.800	0.050
Threshold/Weir crest	3	0.140	0.220 / 0.250	0.030
Abutment	2	0.045	0.545	0.230
Opening	3	0.140	–	–
Sluice gate	3	0.140	0.005	0.100

Source: own work.

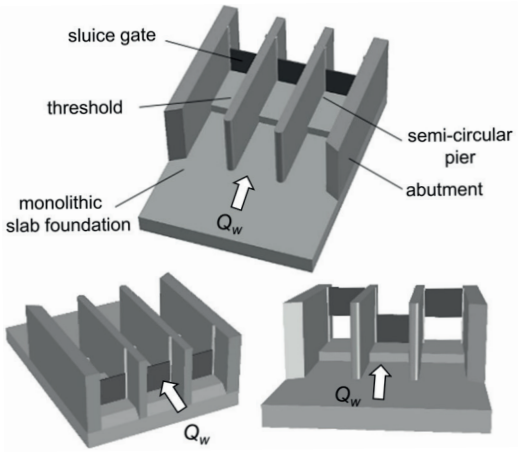

Fig. 4. Conceptual diagram of a laboratory model of the weir

Source: own work.

The primary construction material used for the physical weir model consisted of black and transparent acrylic sheets with thicknesses of 5 mm and 3 mm (Fig. 5a). Acrylic was selected due to its high mechanical strength, resistance to water and humidity, ease of machining to create complex shapes, relatively low cost, and wide availability. All structural walls of the model were precisely cut from acrylic sheets, while PVC tubes were employed to form the rounded edges of the semicircular piers. The components were assembled using acrylic adhesive, forming the skeleton of the foundation slab, abutments, piers, and threshold. After curing, all joints were further sealed with silicone to prevent water ingress into the internal cavities of the model elements.

To enhance rigidity and protect against water penetration, all hollow components were filled with expanding foam (Fig. 5b). Once hardened, the foam was trimmed with a utility knife to achieve a smooth, even surface. Plastic guides for the movable gates were installed on the piers and abutments at a distance of 6.5 cm from the threshold chamfer, allowing precise alignment and vertical adjustment of the sluice gates. Each of the three gates was fabricated from 5 mm acrylic sheet, ensuring a snug fit within the guides. The gates were manually inserted into their guides, enabling water flow both beneath and above the gates during hydraulic testing.

It should be noted that, although the prototype Radomka weir is operated by raising and lowering sluice gates to allow flow beneath them, the laboratory experiments primarily involved overflow over the gates, creating controlled surface overflow conditions. This approach was chosen to create controlled clear-water scour conditions in the laboratory, i.e., with negligible sediment transport in the approach channel, allowing detailed investigation of scour development downstream of the structure. The main reason for using overflow over the gates was that allowing water to flow beneath partially or fully closed sluice gates in a laboratory setup could increase the risk of not achieving clear-water conditions.

Such an approach is widely applied in experimental studies of scour downstream of hydraulic structures. For example, Guan et al. (2019) conducted physical flume tests of local scour downstream of submerged weirs under clear-water scour conditions, illustrating that overflow-driven scour processes can be reliably studied in laboratory models. Similarly, Guan et al. (2016) investigated local scour at submerged weirs in sand-bed channels, confirming that controlled overflow experiments are effective in isolating hydraulic and sedimentary mechanisms. Furthermore, physical model studies of scour downstream of clear over-fall weirs demonstrate that laboratory experiments with overflow are widely accepted for analysing scour processes, even when

the exact operational mechanism of sluice gates is not reproduced (Amin, 2015). Therefore, the laboratory model does not replicate the precise operation of the prototype sluice gates but serves as a simplified, controlled environment to study sediment transport and scour processes under reproducible clear-water conditions.

Fig. 5. Structural elements of the model: a – the frame made of acrylic sheets, b – abutments and pillars filled with expanding foam

Source: own work.

The final stage of model preparation involved coating all structural elements, except for the gates and their guides, with a mixture of paint and sand. This layer served multiple purposes: increasing surface roughness to replicate real hydraulic structures, strengthening the model, and providing a more realistic visual representation of the weir. The model was then left to dry thoroughly.

Prior to installation in the laboratory flume, the bed and walls of the testing facility were carefully cleaned. The model was fixed in place using waterproof adhesive, and any gaps were filled with silicone to prevent water from seeping beneath the structure or along the interfaces between abutments and the flume walls, creating a watertight barrier. Finally, the flume sections upstream and downstream of the structure were filled with erodible sand up to a height of 30 cm to simulate natural sediment conditions during testing (Fig. 6).

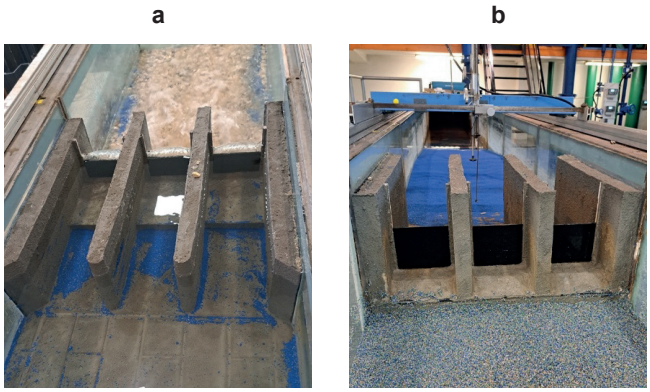

Fig. 6. Physical model of the weir installed in the laboratory flume: a – view from the headwater station, b – view from the tailwater station

Source: own work.

In the laboratory model, no reinforcement was applied to the downstream section. This was an intentional simplification aimed at establishing baseline conditions and enabling the observation of unrestricted scour and sediment transport processes downstream of the weir (Fig. 7). The absence of bed stabilisation allowed for the assessment of the maximum erosion potential and flow-sediment interactions without the influence of protective structures, which are typically present in real weirs. The objective was not to reproduce real-world reinforced conditions, but to isolate the fundamental hydraulic and morphodynamic processes governing scour development.

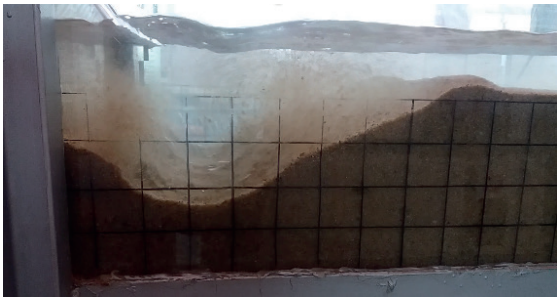

Fig. 7. The local scour phenomenon observed downstream of the weir

Source: own work.

To ensure a reliable representation of sediment properties in laboratory conditions, a detailed granulometric characterisation of the bed material was conducted. Samples from the upper (Sample 1) and lower (Sample 2) model structure stand (Fig. 8), 300 g each, were then subjected to 30-minute tests on a shaker to determine the percentage of fines, and thus the total size range of the aggregate (Fig. 8a). The purpose of using colourful sand was to facilitate observation of the accumulation processes taking place in the upper stand, upstream of the damming object.

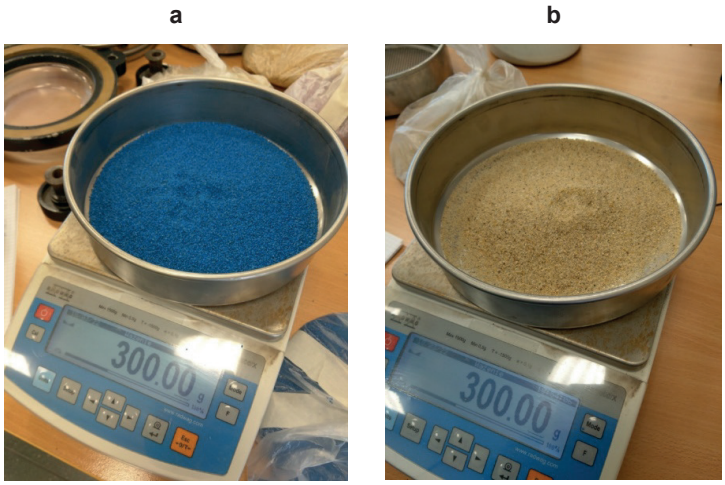

Fig. 8. Soil samples taken from: a – the headwater stand, b – the tailwater stand

Source: own work.

The experimental methodology adhered to standard procedures for soil identification according to PN-EN ISO 14688 (Polski Komitet Normalizacyjny [PKN], 2006), classifying the soil as medium sand with a density of 2.62 g·cm^{-3}. For the arranged grain size curves (Fig. 9), the median diameter was determined, $D_m = D_{50} = 0.95$ mm for the upstream (headwater) and $D_m = D_{50} = 0.49$ mm for the downstream (tailwater). Characteristic diameters of the studied soil were compiled in Table 2, which also summarises the calculated granulometric properties and the comprehensive classification of tested soil samples.

The coefficient of curvature (C_c) of the grain size distribution curve was calculated as follows:

$$C_c = \frac{D_{30}^{\ 2}}{D_{10}D_{60}}. \tag{1}$$

The coefficient of uniformity of grain size distribution (C_u), the so-called Hazen sorting coefficient, was calculated as follows:

$$C_u = \frac{D_{60}}{D_{10}}. \tag{2}$$

The differential grain size index (C_k) according to Knoroz was calculated as follows:

$$C_k = \frac{D_{95}}{D_5}. \tag{3}$$

The dominance coefficient (C_d), reflecting the predominance of grains larger or smaller than the median diameter $D_{50,}$ was calculated as follows:

$$C_d = \frac{D_{90}D_{10}}{D_{50}^{\ 2}}. \tag{4}$$

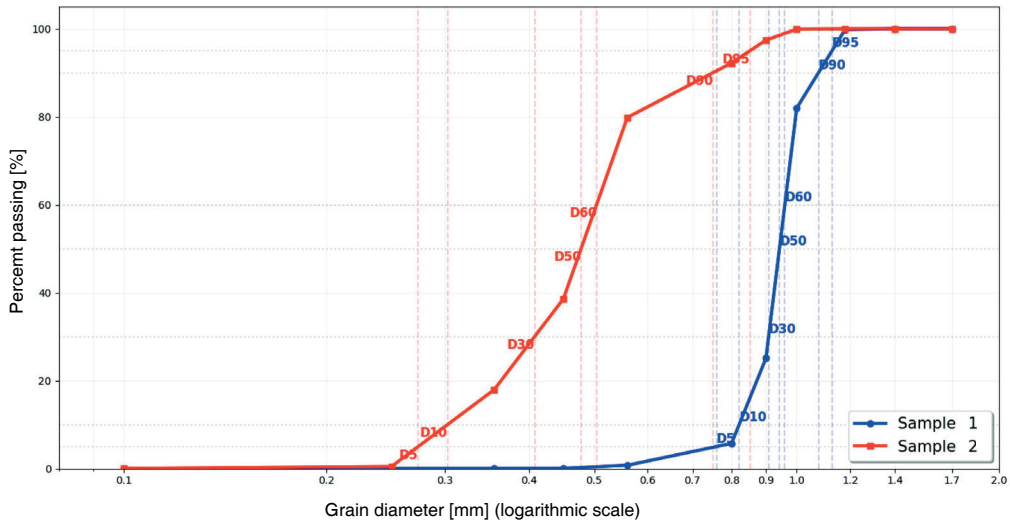

Fig. 9. Grain size curves of bedload grains used in research

Source: own work.

Table 2. Characteristic diameters and granulometric properties of investigated soil samples

Specification	Sample 1	Sample 2	Commentary
	Characteristic diameter [mm]		
$D_m = D_{50}$	0.95	0.49	median diameter
D_5	0.80	0.28	diameter at which 5% of grains are finer
D_{10}	0.85	0.31	diameter at which 10% of grains are finer
D_{30}	0.91	0.41	diameter at which 30% of grains are finer
D_{60}	0.97	0.53	diameter at which 60% of grains are finer
D_{90}	1.06	0.76	diameter at which 90% of grains are finer
D_{95}	1.11	0.85	diameter at which 95% of grains are finer
	Granulometric property [-]		
C_c	1.02	1.01	$C_c \cong 1$ – monofractional material
C_u	1.15	1.70	$C_u < 6$ – monofractional material
C_k	1.40	2.99	$C_k \leq 4$–5 – well-sorted material
C_d	0.98	0.99	$C_d < 1$ – particle diameter smaller than D_{50}

Source: own work.

The characteristic values of the grain size curves provided in Table 2 indicate that coarser bedload with a D_{50} of 0.95 mm was deposited in the upstream reach of the weir, while finer bedload with a D_{50} of 0.49 mm was found in the downstream reach. Both the upstream and downstream bedloads are characterised as monofractional and well sorted. The $C_d < 1$ (particles with a diameter smaller than D_{50}) value for the upstream and for the downstream bedload indicates that bedload finer than D_{50} = 0.95 mm was deposited in the upstream reach, and bedload coarser than D_{50} = 0.49 mm was deposited in the downstream reach.

RESULTS AND DISCUSSION

Temporal evolution of maximum scour depth

Table 3 and Figure 10 demonstrate the evolution of the scour hole depth at successive time steps for each measurement series. The figure is divided into three parts, in which measurement series characterised by similar flow velocities prevailing in the tailwater above the non-scoured bottom are grouped. Each series is therefore described in the legend by the flow velocity value, and the measurement series number is given in brackets, in accordance with Table 2. The scour depth tends to reach its maximum value at the end of the experiment (in 18 out of 25 series).

The evolution of local scour depth over time in the 25 laboratory experiments exhibits patterns characteristic of clear-water conditions. Immediately after the experiment starts, erosion intensity is highest, resulting in a rapid increase in scour depth during the initial 0.5 h. Following this "initial" phase, the rate of erosion gradually slows, and the growth curve of the scour depth flattens out, eventually approaching an asymptotic maximum.

Table 3. Time evolution of maximum local scour depths for each measurement series

Test	Water discharge (Q_w) [$m^3 \cdot s^{-1}$]	Height (h) [m]	Maximum local scour depth (z_{max}) [m]			
			$T = 0$	$T = 0.5$ h	$T = 4.0$ h	$T = 6.0$ h
1	0.0110	0.0440	0.0000	0.1917	0.2609	0.2661
2	0.0121	0.0500	0.0000	0.2248	0.2770	0.2738
3	0.0092	0.0800	0.0000	0.1851	0.2153	0.2211
4	0.0120	0.0500	0.0000	0.2390	0.2790	0.2761
5	0.0092	0.0400	0.0000	0.1761	0.2304	0.2085
6	0.0121	0.0460	0.0000	0.1795	0.2539	0.2654
7	0.0100	0.0500	0.0000	0.1528	0.2357	0.2412
8	0.0077	0.0340	0.0000	0.1590	0.2224	0.2485
9	0.0084	0.0490	0.0000	0.1880	0.1900	0.1966
10	0.0119	0.0450	0.0000	0.2310	0.2688	0.2693
11	0.0085	0.0400	0.0000	0.2130	0.2403	0.2330
12	0.0100	0.0440	0.0000	0.2038	0.2160	0.2320
13	0.0150	0.0500	0.0000	0.2045	0.2366	0.2580
14	0.0150	0.0800	0.0000	0.1922	0.2021	0.2210
15	0.0200	0.0500	0.0000	0.2765	0.2646	0.2880
16	0.0200	0.0520	0.0000	0.2579	0.2544	0.2760
17	0.0250	0.0660	0.0000	0.2652	0.2552	0.2820
18	0.0250	0.0650	0.0000	0.2803	0.2957	0.2840
19	0.0230	0.0640	0.0000	0.2558	0.2842	0.2710
20	0.0201	0.0540	0.0000	0.2461	0.2535	0.2810
21	0.0211	0.0550	0.0000	0.2410	0.2571	0.2790
22	0.0211	0.0610	0.0000	0.2296	0.2684	0.2680
23	0.0130	0.0540	0.0000	0.2218	0.2428	0.2460
24	0.0150	0.0590	0.0000	0.2184	0.2233	0.2420
25	0.0110	0.0430	0.0000	0.2296	0.2536	0.2550

Source: own work.

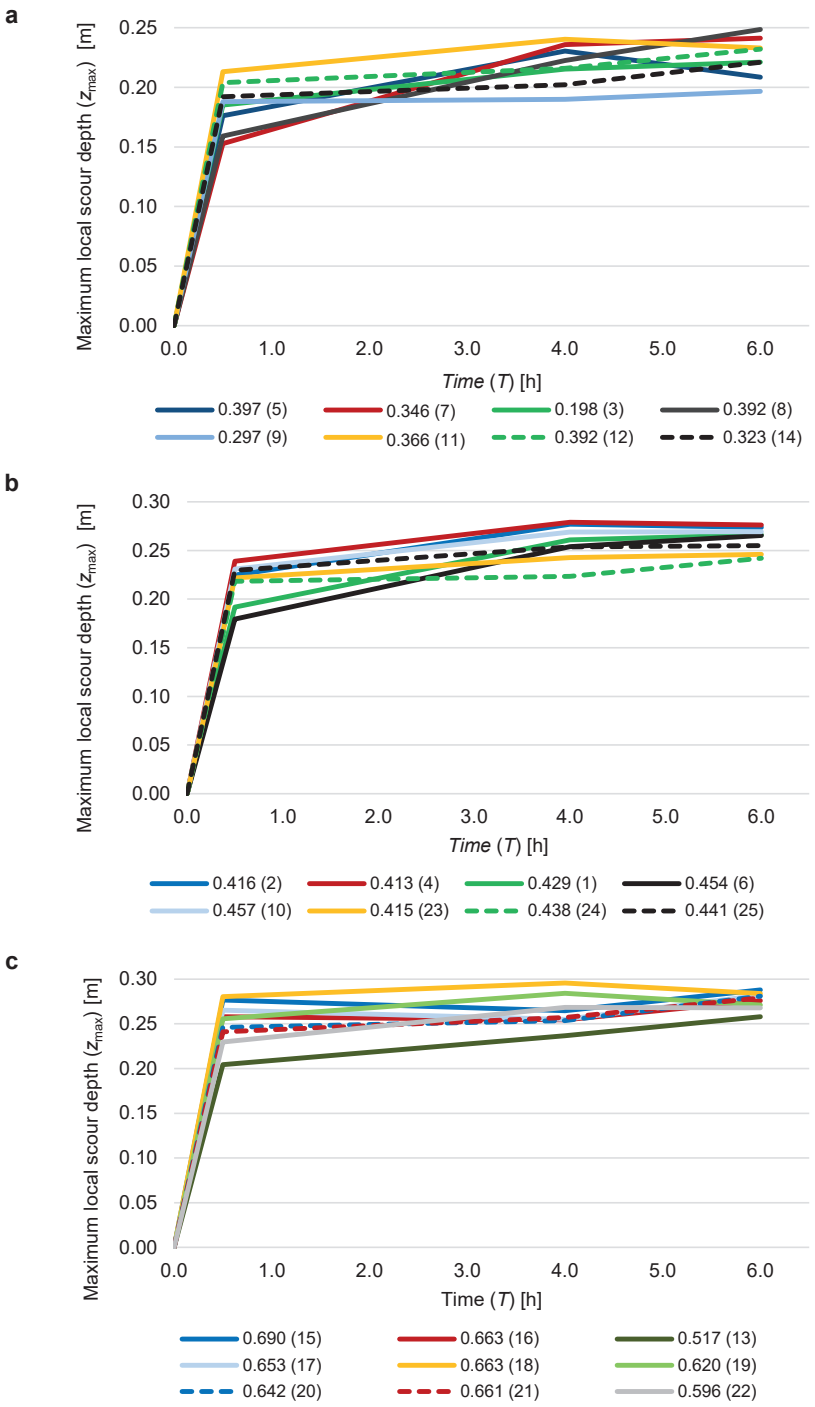

Fig. 10. Evolution of maximum local scour depths over time for each measurement series, described by downstream flow velocities ranges: a – 0.200–0.390 m·s^{-1}, b – 0.410–0.460 m·s^{-1}, c – 0.520–0.690 m·s^{-1}

Source: own work.

Table 4 presents the evolution of local scour depth as a percentage of the maximum observed depth for all 25 laboratory series at different time steps: 0.5 h, 4.0 h, and 6.0 h. Each experimental series was additionally characterised by the flow velocity measured in the downstream section above the non-erodible bed. Several clear patterns can be observed.

Table 4. Temporal evolution of scour depth expressed as percentage of the maximum value

Test	Flow velocity (v) [m·s^{-1}]	Maximum local scour depth (z_{max})		
		0.5 h	4.0 h	6.0 h
		% of six-hour experiment		
1	0.429	72.0	98.0	100
2	0.416	82.1	101.2	100
3	0.198	83.7	97.4	100
4	0.413	86.6	101.0	100
5	0.397	84.5	110.5	100
6	0.454	67.6	95.7	100
7	0.346	63.4	97.7	100
8	0.392	64.0	89.5	100
9	0.297	95.6	96.6	100
10	0.457	85.8	99.8	100
11	0.366	91.4	103.1	100
12	0.392	87.8	93.1	100
13	0.517	87.8	93.1	100
14	0.323	79.3	91.7	100
15	0.690	87.0	91.4	100
16	0.663	96.0	91.9	100
17	0.653	93.4	92.2	100
18	0.663	94.0	90.5	100
19	0.620	98.7	104.1	100
20	0.642	94.4	104.9	100
21	0.661	87.6	90.2	100
22	0.596	86.4	92.2	100
23	0.415	85.7	100.1	100
24	0.438	90.2	98.7	100
25	0.441	90.2	92.3	100

Source: own work.

Across almost all series, a significant proportion of the maximum scour depth is reached within the first 0.5 h. In the present analysis, the maximum scour depth was defined as the value measured after 6.0 h of the experiment. This assumption was adopted because scour development in most series approached a stable state by that time, and further changes in depth were relatively small.

In most cases, 63–96% of the maximum depth is achieved during this early phase. This indicates a highly active initial erosion phase consistent with clear-water scour, where the undisturbed sediment near the obstacle is quickly mobilised by the incoming flow. Between 0.5 h and 4.0 h, the rate of scour depth increase slows down, reflecting the gradual depletion of easily erodible sediment around the obstacle. By 4.0 h, most series have already reached 90–105% of the maximum depth.

Based on the percentage values presented in the table, the average scour depth reached after 0.5 h corresponds to 85.4% of the final depth observed after 6.0 h. This indicates that a very significant part of the scour development occurs during the initial stage of the experiment. After 4.0 h, the average scour depth reaches 96.4% of the final depth. This demonstrates that the scour process significantly slows down after the initial stage and gradually approaches its final equilibrium value. The obtained values prove that regardless of absolute depth values, the temporal evolution is similar across series: rapid early erosion, slowing approach to maximum, and stabilisation around the final scour depth.

A comparison of the velocity values with the percentage of the final scour depth reached after 0.5 h indicates a clear relationship between flow velocity and the rate of scour development. Experiments conducted at higher velocities, typically in the range of 0.60–0.69 $m \cdot s^{-1}$, reached more than 90% of the final scour depth within the first 0.5 h. In contrast, experiments with lower velocities, around 0.20–0.35 $m \cdot s^{-1}$, reached only about 60–80% of the final depth in the same period. This trend suggests a positive correlation between flow velocity and the rate of scour growth, particularly during the initial phase of the process, when erosion intensity is highest.

The Pearson correlation coefficient between velocity and the percentage of the final scour depth reached after 0.5 h equals 0.43, indicating a moderate positive correlation (Fig. 11). This suggests that higher flow velocities generally lead to a faster initial development of the scour hole. However, when the same analysis is performed for the scour depth after 4.0 h, the correlation coefficient decreases to −0.26, indicating a very weak relationship.

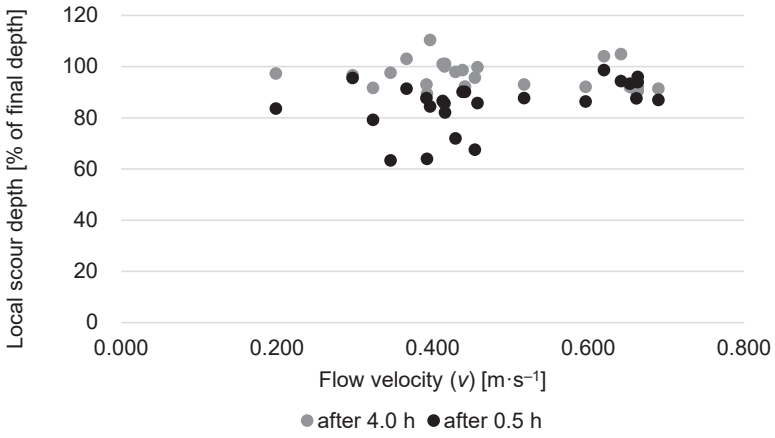

Fig. 11. Relationship between flow velocity and scour development over time

Source: own work.

This result shows that the influence of flow velocity on the rate of scour development is most pronounced during the initial phase of the process. At later stages, the scour depth approaches its final equilibrium value, and the influence of velocity on further growth becomes much less significant.

Temporal distribution of scour depth increments

To analyse the dynamics of scour development around the structure, changes in scour depth were evaluated over successive time intervals of the experiment (Fig. 12). For each measurement series, the maximum scour depth increment (Δz_{max}) was defined as the largest increase in scour depth recorded between consecutive measurements during the six-hour experimental run. Scour depth increments were determined for three characteristic time intervals: from the start of the experiment to 0.5 h ($\Delta T_{0–0.5\,h}$), from 0.5 h to 4.0 h ($\Delta T_{0.5–4.0\,h}$), and from 4.0 h to 6.0 h ($\Delta T_{4.0–6.0\,h}$). The cumulative development of scour depth averaged for all experimental series shows a very rapid initial growth of the scour hole. Within the first 0.5 h the mean scour depth reaches about 0.219 m, which corresponds to about 86% of the final depth measured after 6.0 h. After 4.0 h the mean depth increases only slightly to about 0.247 m (about 97% of the final value). Further evolution between 4.0 h and 6.0 h is minimal, indicating that the scour process approaches equilibrium conditions relatively quickly (Fig. 13).

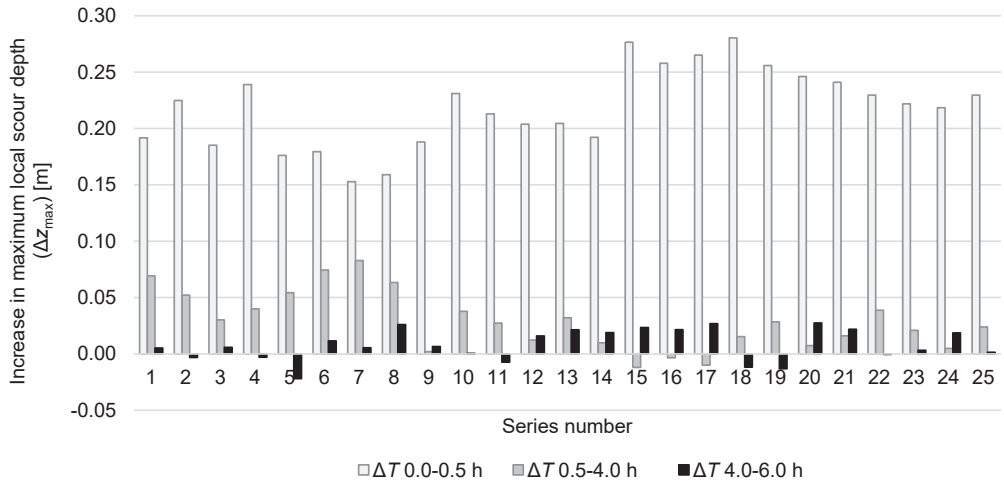

Fig. 12. Temporal distribution of scour depth increments during the six-hour experiment

Source: own work.

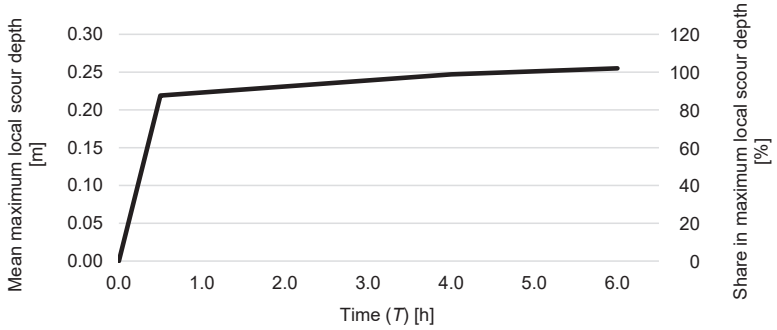

Fig. 13. Temporal evolution of the averaged maximum local scour depth from 25 measurement series

Source: own work.

The obtained results confirm the typical pattern of local scour development observed in laboratory studies, where the majority of the final scour depth forms during the initial period of flow action, while the subsequent evolution of the erosional feature is characterised by gradual stabilisation of the scour geometry.

Scour development rate

To analyse the dynamics of scour evolution, the scour development rate was calculated for three characteristic phases of the experiment. The rate was defined as the increase in scour depth within a given time interval divided by the duration of that interval:

$$R_1 = \frac{\Delta z_{0–0.5\ \mathrm{h}}}{0.5\ \mathrm{h}}. \tag{5}$$

$$R_2 = \frac{\Delta z_{0.5–4.0\ \mathrm{h}}}{3.5\mathrm{h}}. \tag{6}$$

$$R_3 = \frac{\Delta z_{4.0–6.0\ \mathrm{h}}}{2.0\ \mathrm{h}}. \tag{7}$$

where:
R_1, R_2, R_3 – scour development rates for successive phases of the experiment [m·h^{-1}],
$\Delta z_{0–0.5\ \mathrm{h}}$ – scour increase during the first 0.5 h [m],
$\Delta z_{0.5–4.0\ \mathrm{h}}$ – scour increase between 0.5 h and 4.0 h [m],
$\Delta z_{4.0–6.0\ \mathrm{h}}$ – scour increase between 4.0 h and 6.0 h [m].

The calculated rates represent the erosion velocity, expressed either in m·h^{-1} or m·s^{-1} (Table 5). The average values obtained from all 25 experimental series indicate strong temporal variability of the scour development rate (Fig. 14). During the initial phase of the experiment (0–0.5 h), the mean scour rate reached 0.437 m·h^{-1}, which corresponds to about 1.2×10^{-6} m·s^{-1}. In the intermediate phase (0.5–4.0 h), the average rate decreased significantly to 0.00821 m·h^{-1} (about 2.28×10^{-6} m·s^{-1}). During the final stage of the experiment (4.0–6.0 h), the scour development rate was even lower, reaching an average value of 0.00403 m·h^{-1}, equivalent to about 1.12×10^{-6} m·s^{-1}.

Table 5. Scour development rate in particular phases

Test	R_1	R_2	R_3	R_1	R_2	R_3
		m·h^{-1}			×10^6 m·s^{-1}	
1	0.3834	0.0198	0.0026	1.065	0.055	0.007
2	0.4496	0.0149	−0.0016	1.249	0.041	−0.004
3	0.3702	0.0086	0.0029	1.028	0.024	0.008
4	0.4780	0.0114	−0.0015	1.328	0.032	−0.004
5	0.3522	0.0155	−0.0110	0.978	0.043	−0.030
6	0.3590	0.0213	0.0058	0.997	0.059	0.016
7	0.3056	0.0237	0.0028	0.849	0.066	0.008
8	0.3180	0.0181	0.0131	0.883	0.050	0.036
9	0.3760	0.0006	0.0033	1.044	0.002	0.009
10	0.4620	0.0108	0.0003	1.283	0.030	0.001

Table 5 (cont.)

Test	R_1	R_2	R_3	R_1	R_2	R_3
		$m \cdot h^{-1}$			$\times 10^6\ m \cdot s^{-1}$	
11	0.4260	0.0078	−0.0037	1.183	0.022	−0.010
12	0.4076	0.0035	0.0080	1.132	0.010	0.022
13	0.4090	0.0092	0.0107	1.136	0.025	0.030
14	0.3844	0.0028	0.0095	1.068	0.008	0.026
15	0.5530	−0.0034	0.0117	1.536	−0.009	0.033
16	0.5158	−0.0010	0.0108	1.433	−0.003	0.030
17	0.5304	−0.0029	0.0134	1.473	−0.008	0.037
18	0.5606	0.0044	−0.0059	1.557	0.012	−0.016
19	0.5116	0.0081	−0.0066	1.421	0.023	−0.018
20	0.4922	0.0021	0.0138	1.367	0.006	0.038
21	0.4820	0.0046	0.0110	1.339	0.013	0.030
22	0.4592	0.0111	−0.0002	1.276	0.031	−0.001
23	0.4436	0.0060	0.0016	1.232	0.017	0.004
24	0.4368	0.0014	0.0094	1.213	0.004	0.026
25	0.4592	0.0069	0.0007	1.276	0.019	0.002
Mean	0.4370	0.0082	0.0040	1.214	0.023	0.011

Source: own work.

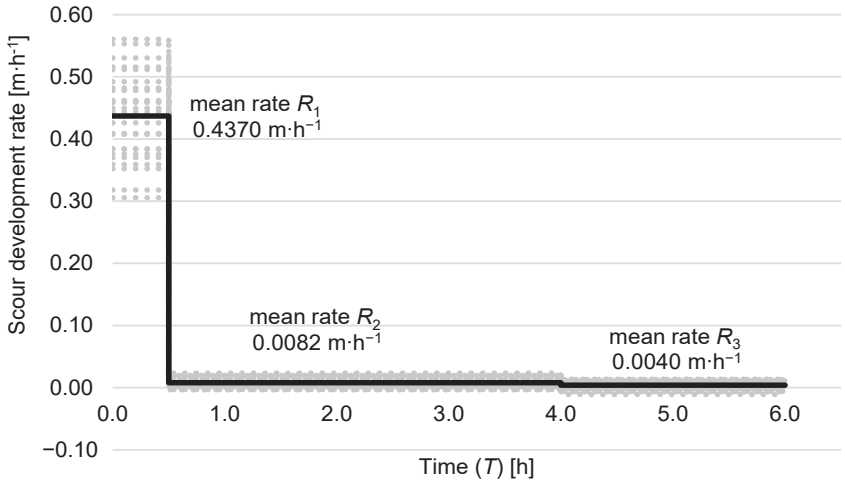

Fig. 14. Scour development rate over time

Source: own work.

The results show very strong temporal variability in scour intensity. The erosion rate during the initial phase of the experiment is about 53 times greater than during the intermediate phase (0.5–4.0 h) and over 100 times greater than during the final phase (4.0–6.0 h).

Phase contribution to final scour depth

In order to quantify the relative importance of each stage in the scour development process, the phase contribution coefficient (C_i) was introduced (Table 6). It represents the proportion of the final scour depth formed during a given time interval and is defined as:

$$C_i = \frac{\Delta z_i}{z_{\max}}. \tag{8}$$

where:
C_i – the contribution of Phase i [%],
Δz_i – the increase in scour depth during Phase i [m],
$z_{\max}$ – the final scour depth measured after 6.0 h of the experiment [m].

The average phase contributions calculated for all experimental series indicate that the majority of scour development occurred during the initial stage of the experiment. The phase between 0 and 0.5 h accounts on average for about 85.5% of the final scour depth. The intermediate phase between 0.5 h and 4.0 h contributes about 11.4%, while the final phase between 4.0 h and 6.0 h represents only about 3.1% of the total scour depth.

The relative contribution of each phase (C_1, C_2, and C_3) to the total scour depth is presented in Figure 15. The box-and-whisker plot illustrates the dominance of Phase C_1, which accounts for a median value of 87.0% of the total process. The narrow interquartile range for C_1 suggests high consistency across the experimental series, although several outliers (represented by open circles) indicate instances where its contribution dropped to 63.0–72.0%.

Table 6. Phase contribution to final scour depth

Test	C_1	C_2	C_3	Test	C_1	C_2	C_3
	%				%		
1	72.0	26.0	2.0	14	87.0	4.5	8.6
2	82.1	19.1	−1.2	15	96.0	−4.1	8.1
3	83.7	13.7	2.6	16	93.4	−1.3	7.8
4	86.6	14.5	−1.1	17	94.0	−3.5	9.5
5	84.5	26.0	−10.5	18	98.7	5.4	−4.1
6	67.6	28.0	4.3	19	94.4	10.5	−4.9
7	63.3	34.4	2.3	20	87.6	2.6	9.8
8	64.0	25.5	10.5	21	86.4	5.8	7.8
9	95.6	1.0	3.4	22	85.7	14.5	−0.1
10	85.8	14.0	0.2	23	90.2	8.5	1.3
11	91.4	11.7	−3.1	24	90.2	2.0	7.7
12	87.8	5.3	6.9	25	90.0	9.4	0.5
13	79.3	12.4	8.3	Mean	85.5	11.4	3.1

Source: own work.

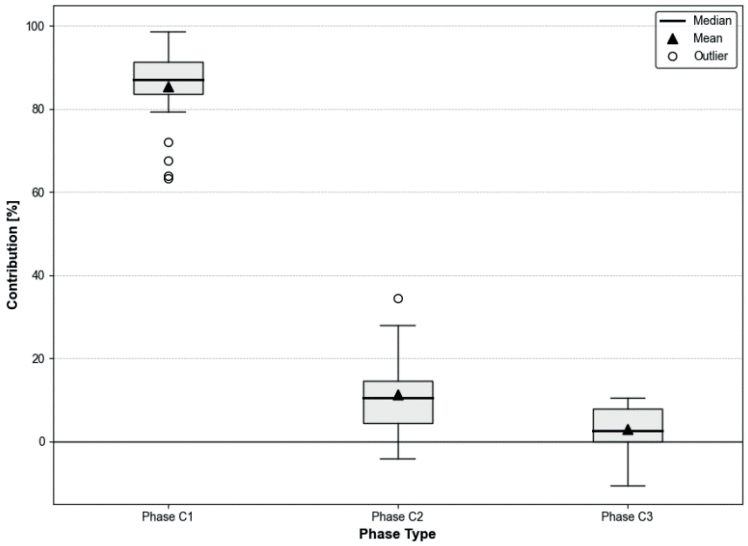

Fig. 15. Distribution of phase contribution to final scour depth

Source: own work.

In contrast, Phases C_2 and C_3 show significantly lower impact, with median values of 11.7% and 2.6%, respectively. Notably, Phase C_2 exhibits the highest variability, with contributions reaching up to 34.4%. The presence of negative outliers in Phases C_2 and C_3 (falling below the 0% threshold) highlights specific conditions where these phases resulted in local sediment accumulation rather than further erosion. The mean values (indicated by black triangles) remain closely aligned with the medians, suggesting a relatively balanced distribution of results within each phase, despite the presence of extreme observations.

CONCLUSIONS

The laboratory experiments conducted on a scaled physical model of a weir on the Radomka provided detailed insights into the temporal evolution of local scour under clear-water conditions. The results confirmed that the scour process downstream of hydraulic structures is strongly time-dependent and dominated by an initial rapid erosion phase. Across all 25 experimental series, the majority of the final scour depth (85.5% on average) was formed within the first 0.5 h of the experiment, demonstrating that local bed material near the weir is highly susceptible to immediate mobilisation by the high-energy jet. The pattern observed, with a rapid initial increase followed by slowing growth approaching an asymptotic maximum, is typical of clear-water conditions, where the flow lacks significant suspended sediment and erosion is primarily controlled by flow velocity and obstacle geometry.

Following the initial stage, the rate of scour development decreased markedly. The intermediate phase (0.5–4.0 h) contributed approximately 11.4% to the final scour depth, while the final stage (4.0–6.0 h) accounted for only 3.1%. This temporal distribution highlights the strong variability in erosion intensity, with the initial phase exhibiting a scour rate over 50 times higher than later phases.

The analysis also revealed a moderate positive correlation between downstream flow velocity and the early rate of scour development, indicating that higher velocities accelerate the formation of the scour hole.

However, as the scour depth approaches equilibrium, the influence of flow velocity diminishes, and the bed gradually stabilises around its final depth.

Overall, the study confirms the classical pattern of clear-water scour: rapid initial erosion, followed by gradual stabilisation and approach to equilibrium. These results provide quantitative insights into the timing, magnitude, and dynamics of local scour, enabling more accurate predictions of scour depth, better assessment of structural safety, and more effective design of bed protection measures downstream of weirs.

Acknowledgements

The materials used for the construction of the physical model of the weir were financed within the research project "Local scour modelling in the region of small hydraulic structures", funded by the Miniatura 4 programme of the National Science Centre (NCN), Poland (2020–2021).

The author would also like to acknowledge the valuable contribution and active participation of students from the Civil Engineering, Environmental Engineering, and Water Engineering and Management programmes who participated in conducting the experiment: A. Kluj, M. Sieczych, M. Naliwajko, J. Górka, K. Dybała, K. Grodzki, M. Wiewiórka, M. Żurawska, K. Gajda, M. Urbanek.

Authors' contributions

Conceptualisation: M.K.; methodology: M.K.; validation: J.G. and M.K.; formal analysis: J.G.; investigation: J.G.; resources: M.K.; data curation: J.G.; writing – original draft preparation: J.G.; writing – review and editing: J.G. and M.K.; visualisation: M.K.; supervision: M.K.; project administration: M.K.; funding acquisition: M.K.

All authors have read and agreed to the published version of the manuscript.

REFERENCES

Amin, A. M. A. (2015). Physical model study for mitigating local scour downstream of clear over-fall weirs. *Ain Shams Engineering Journal*, *6*(4), 1143–1150. https://doi.org/10.1016/j.asej.2015.03.013

Brath, A., & Montanari, A. (2000). Temporal evolution of local scour at bridge piers. *Journal of Hydraulic Engineering*, *126*(10), 778–782.

Ghani, A. A., & Mohammadpour, R. (2016). Temporal variation of clear-water scour at compound abutments. *Ain Shams Engineering Journal*, *7*(4), 1045–1052.

Graf, W. H. (1998). *Fluvial hydraulics: flow and transport processes in channels of simple geometry*. John Wiley & Sons.

Guan, D., Liu, J., Chiew, Y.-M., & Zhou, Y. (2019). Scour evolution downstream of submerged weirs in clear water scour conditions. *Water*, *11*(9). https://doi.org/10.3390/w11091746

Guan, D., Melville, B., & Friedrich, H. (2014). Flow patterns and turbulence structures in a scour hole downstream of a submerged weir. *Journal of Hydraulic Engineering*, *140*(1), 68–76. https://doi.org/10.1061/(ASCE)HY.1943-7900.0000803

Guan, D., Melville, B., & Friedrich, H. (2016). Local scour at submerged weirs in sand-bed channels. *Journal of Hydraulic Research*, *54*(2), 172–184. https://doi.org/10.1080/00221686.2015.1132275

Hopfinger, E. J., Kurniawan, A., Graf, W. H., & Lemmin, U. (2004). Sediment erosion by Görtler vortices: The scour-hole problem. *Journal of Fluid Mechanics*, *520*, 327–342. https://doi.org/10.1017/S0022112004001636

İkincioğulları, E., Emiroğlu, M. E., & Aydın, M. C. (2026). Investigation of local scour at classical contracted rectangular weir downstream using CFD. *Firat University Journal of Experimental and Computational Engineering*, *5*(1), 231–249. https://doi.org/10.62520/fujece.1804990

Kiraga, M., Bajkowski, S., Urbański, J., & Siwicki, P. (2025). Experimental studies on the local scour development of the riverbed below the Piaseczno Weir. *Water*, *17*(13), 1916. https://doi.org/10.3390/w17131916

Lantz, W. D., Crookston, B. M., & Palermo, M. (2022). Evolution of local scour downstream of Type A PK weir in non-cohesive sediments. *Journal of Hydrology and Hydromechanics*, *70*(1), 103–113. https://doi.org/10.2478/johh-2021-0035

Majewska, L. (2025). *Zmiany ukształtowania laboratoryjnego dna aluwialnego w warunkach przepływu ustalonego* [*Analysis of morphological alterations in laboratory alluvial bed during steady-state flow conditions*] (Bachelor's thesis). Szkoła Główna Gospodarstwa Wiejskiego w Warszawie.

Millar, B., Hamill, G., Taylor, S., & Robinson, D. (2024). ArchIMEDES: Computer vision tracking of the inherent changes to structural stability of masonry arch bridges resulting from increased bed scour. *e-Journal of Nondestructive Testing*, *29*(7). https://doi.org/10.58286/29586

Panthi, M., Crookston, B. M., & Palermo, M. (2026). Scour evolution for steady and unsteady flow conditions downstream of Type A piano key weirs. *Journal of Hydrology and Hydromechanics*, *74*(1), 20–35. https://doi.org/10.2478/johh-2026-0003

Polski Komitet Normalizacyjny [PKN]. (2006). *Badania geotechniczne. Oznaczanie i klasyfikowanie gruntów* [*Geotechnical investigation and testing. Identification and classification of soil*] (PN-EN ISO 14688).

Tunas, M., Benmebarek, N., & Mohammed, A. (2024). Numerical investigation of local scour downstream of a weir. *International Journal of Safety and Security Engineering*, *14*(2), 359–370. https://doi.org/10.18280/ijsse.140220

Wang, L., Lu, W., Melville, B., Guan, D., & Whittaker, C. (2018). Local scour at downstream sloped submerged weirs. *Journal of Hydraulic Engineering*, *144*, 04018029. https://doi.org/10.1061/(ASCE)HY.1943-7900.0001492

Zhang, W., Nie, R., Liu, X.., Yang, S., & Wang, L. (2025). Clear-water scour depth at rock weirs under unsteady flows. *Journal of Hydrology*, *654*, 132889. https://doi.org/10.1016/j.jhydrol.2025.132889

ROZWÓJ ROZMYCIA LOKALNEGO W CZASIE W WARUNKACH NAPŁYWU WODY POZBAWIONEJ RUMOWISKA PONIŻEJ JAZU

STRESZCZENIE

Celem pracy była analiza ewolucji czasowej rozmycia lokalnego poniżej jazu, gdy napływająca woda nie niesie rumowiska. Postawiono hipotezę, że większość rozmycia powstaje w fazie początkowej przepływu, a tempo jego rozwoju zależy od prędkości przepływu poniżej budowli. Badania przeprowadzono w warunkach laboratoryjnych na modelu fizycznym jazu w skali 1 : 30, odwzorowującym rzeczywiste warunki hydrauliczne i sedymentacyjne. Wykazano, że średnio 85–86% głębokości maksymalnej rozmycia powstaje w ciągu pierwszej 0,5 godziny eksperymentu, natomiast w kolejnych etapach tempo erozji wyraźnie maleje i stabilizuje się w pobliżu wartości końcowej. Większe prędkości przepływu przyspieszają początkowy rozwój rozmycia, jednak ich wpływ na dalsze etapy procesu jest znacznie mniejszy. Uzyskane wyniki potwierdzają typowy przebieg rozwoju rozmycia, gdy napływająca woda nie niesie rumowiska, a wnioski z badania mogą być wykorzystane przy ocenie bezpieczeństwa budowli hydrotechnicznych oraz projektowaniu zabezpieczeń dna poniżej jazów.

Słowa kluczowe: rozmycie lokalne, jaz, rozwój rozmycia w czasie, model fizyczny, budowla hydrotechniczna